Title

Immune complex relay by subcapsular sinus macrophages and noncognate B cells drives antibody affinity maturation.

Journal

Nature immunology, 10(7)

ISSN

1529-2908

Authors

Phan, Tri Giang
Green, Jesse A
Gray, Elizabeth E
et al.

Publication Date

2009-07-01

DOI

10.1038/ni.1745

Peer reviewed

HHS Public Access

Author manuscript

Nat Immunol. Author manuscript; available in PMC 2010 January 01.

Published in final edited form as:

Nat Immunol. 2009 July ; 10(7): 786–793. doi:10.1038/ni.1745.

Immune complex relay by subcapsular sinus macrophages and non-cognate B cells drives antibody affinity maturation

Tri Giang Phan[1,2], **Jesse A. Green**[1,*], **Elizabeth E. Gray**[1,*], **Ying Xu**[1], and **Jason G. Cyster**[1]

[1]Howard Hughes Medical Institute and Department of Microbiology and Immunology, University of California San Francisco, CA 94143, USA

[2]Garvan Institute of Medical Research, 384 Victoria St Darlinghurst, Sydney NSW 2010, Australia

Abstract

Subcapsular sinus (SCS) macrophages capture antigens from lymph and present them intact for B cell encounter and follicular delivery. However, the properties of SCS macrophages are poorly defined. Here we show SCS macrophage development depended on lymphotoxin-α1β2 and the cells had low lysosomal enzyme expression and retained opsonized antigens on their surface. Intravital imaging revealed immune complexes moving along macrophage processes into the follicle. Moreover, non-cognate B cells relayed antigen opsonized by newly produced antibodies from the subcapsular sinus to the germinal center and affinity maturation was impaired when this transport process was disrupted. Thus, we characterize SCS macrophages as specialized antigen-presenting cells functioning at the apex of an antigen transport chain that promotes humoral immunity.

Early studies tracking the fate of opsonized antigens arriving in lymph nodes showed that large amounts of antigen were trapped and catabolized by macrophages in the medulla, while smaller amounts were captured by macrophages lining the subcapsular sinus (SCS)1–3. Previous studies have demonstrated that SCS macrophages efficiently capture several types of particulate antigen and facilitate their display for cognate recognition by follicular B cells4–6. In one study it was shown that immune complexes (ICs) could be captured from SCS macrophages by non-cognate B cells via complement receptors 1 and 2 (CR1/2) [http://www.signaling-gateway.org/molecule/query?afcsid=A000541], and these cells mediated IC delivery to follicular dendritic cells (FDCs) in primary follicles5. SCS macrophages thus have an established role as antigen-presenting cells for B cells. However, in contrast with the wealth of information available regarding dendritic cells, the antigen-presenting cells of the T zone7, SCS macrophages have not been isolated in pure form and little is known about their cell biological properties or developmental requirements.

In a primary immune response, initial antibody secretion occurs within 3–5 days and the germinal center (GC) response peaks several days later8. The GC is characterized as a site

Correspondence should be addressed to Tri Giang Phan (t.phan@garvan.org.au), and Jason G. Cyster (Jason.Cyster@ucsf.edu).
*These authors contributed equally to this work

where newly mutated B cells compete for antigen, allowing selection events to occur that lead to antibody affinity maturation9. ICs are displayed within GCs, particularly on light zone FDCs, but GCs have generally been thought to exclude follicular B cells and the mechanism of IC delivery to GCs has not been established. However, recent real-time imaging studies have provided evidence that follicular B cells can indeed access the GC light zone10, 11, raising the possibility that IC relay is involved in delivery of antigen and newly formed antibody to GCs.

Here we use surface phenotyping of isolated cells to distinguish SCS macrophages from two populations of medullary macrophages. SCS macrophages were smaller and had lower expression of lysosomal enzymes. SCS macrophages displayed ICs on their surface and delivered complexes unidirectionally along processes that extended into the follicle. These cells were dependent on the cytokine lymphotoxin derived from B cells for their development and function. Disruption of the IC relay from SCS macrophages to FDC by removing CR1/2 from non-cognate B cells led to a reduction in antibody affinity maturation, establishing a role for IC relay in driving the GC response.

Results

Isolation and identification of SCS macrophages

Based on *in situ* staining, both SCS and medullary macrophages expressed the sialic acid-binding immunoglobulin-like C-type lectin sialoadhesin (CD169) recognized by the monoclonal antibodies (mAbs) Ser-4 and MOMA-1 (12 and Fig. 1a). However, $CD169^+$ macrophages lining the SCS can be distinguished from those lining the medullary sinuses in lymph node sections by their lack of staining with the F4/80 mAb (13 and Fig. 1a). To isolate and identify SCS macrophages we digested lymph nodes with a protease cocktail and stained single cell suspensions with mAbs to CD11b (CR3, also called Mac1), CD11c (CR4), CD169 and F4/80 antigen for flow cytometry. This analysis revealed distinct populations of $CD11b^+$ $CD11c^{lo}$ macrophages and $CD11b^+$ $CD11c^{hi}$ classical dendritic cells (Fig. 1b). We excluded $CD11c^{hi}$ cells from our analysis as macrophages lining the SCS and medullary sinuses have low to undetectable levels of this marker by immunofluorescence microscopy in contrast to the bright staining of classical dendritic cells residing in the T zone (Supplementary Fig. 1 online). Further analysis of total $CD11b^+$ $CD11c^{lo}$ macrophages for expression of CD169 and F4/80 antigen revealed the $CD169^{hi}$ cells could be divided into F4/80-negative and -positive subsets as well as a third macrophage population that was $CD169^-$ $F4/80^+$ (Fig. 1b). Immunofluorescence analysis of lymph node sections showed that both $CD169^{hi}$ $F4/80^+$ and $CD169^-$ $F4/80^+$ populations resided in lymph node medullary regions (Fig. 1a). Using an alternative gating scheme, it was possible to identify the SCS-lining macrophages as $CD169^{hi}$ $CD11c^{lo}$ cells that express CD11b and were negative for F4/80 antigen (Fig. 1c). In subsequent experiments we utilized the $CD169^{hi}$ $CD11c^{lo}$ gating strategy and thus focused our attention on a comparison of the $CD169^{hi}$ $F4/80^-$ and the $CD169^{hi}$ $F4/80^+$ macrophage subsets. Light scatter analysis showed the $F4/80^-$ subset was smaller and less granular than the $F4/80^+$ subset (Fig. 1d). We next asked if these cells were able to capture *in vivo* generated ICs containing the fluorescent dye phycoerythrin (PE)5. Both $CD169^{hi}$ macrophage subsets became heavily labeled with PE-ICs 2 h following PE

injection in rabbit IgG anti-PE passively immunized mice, with the F4/80^{+} medullary cells showing substantially higher labeling (Fig. 1e,f) and *in vitro* mixing experiments confirmed that the PE-IC capture occurred *in vivo* rather than during cell isolation (Fig. 1e). In contrast, there was no PE-IC labeling of CD169^{-} F4/80^{+} cells (data not shown). Thus, we could isolate and identify IC-capturing SCS macrophages as CD169^{hi} CD11c^{lo} CD11b^{+} F4/80^{-} cells.

SCS macrophages are poorly endocytic and degradative

To investigate the handling of captured ICs by SCS and medullary macrophages we harvested lymph nodes 4 h after PE injection and stripped surface-bound molecules with acetic acid. Remarkably, acid stripping removed almost all the PE-ICs from the surface of the SCS macrophages without severely affecting the labeling of the medullary population (Fig. 2a,b). As another approach to test for PE-IC internalization, we stained draining lymph node macrophages with antibody against rabbit IgG to detect the passively transferred PE-specific antibody (Fig. 2c). This analysis showed that SCS macrophages had lower amounts of PE-ICs that were protected from anti-rabbit IgG surface staining and therefore presumably located intracellularly (Fig. 2c,d). To determine the fate of internalized ICs, we modified the above protocol and treated mice with an antigen that increases in fluorescence following degradation. Mice were given Alexa Fluor 647-labeled bovine serum albumin-(BSA-) specific polyclonal rabbit IgG and then subcutaneously injected with self-quenching DQ Green BSA extensively haptenated with 4,4-difluoro-5,7-dimethyl-4-bora-3a,4a-diaza-*s*-indacene-3-propionic acid fluorophore (BODIPY FL) to generate BSA–anti-BSA ICs. Following internalization and degradation in lysosomes, the DQ Green BSA is hydrolyzed to single dye-labeled peptides that fluoresce in the green channel. Such fluorescence was readily observed in medullary but not SCS macrophage populations (Fig. 2e). To account for the differential capture of ICs we compared SCS and medullary macrophages with low, intermediate and high labeling with BSA-specific Alexa Fluor 647-labeled rabbit IgG for the production of green fluorescence (Fig. 2e). This analysis showed that for the same amount of IC capture, medullary macrophages consistently degraded more BSA than SCS macrophages. Taken together these findings suggest that SCS macrophages are a poorly endocytic macrophage population with low degradative capacity that retains ICs on the cell surface whereas medullary macrophages capture larger amounts of ICs and are highly endocytic.

SCS macrophages translocate ICs along cellular processes

We then performed intravital two-photon microscopy to image the handling of ICs by SCS macrophages *in vivo*. To label sinus-lining macrophages we subcutaneously injected Alexa Fluor 488-conjugated CD169-specific mAb the day before imaging. B cells expressing the reporter cyan fluorescent protein (CFP) were adoptively transferred to delineate lymphoid follicles. Lymph in the SCS in these experiments was clearly visible as granular autofluorescent green material flowing in the space between the blue collagen second harmonic signal from the capsule and the green layer of labeled macrophages lining the floor of the SCS (Supplementary Movie 1 online). Following injection of PE into mice passively immunized with PE-specific rabbit polyclonal antibodies, we observed rapid drainage of PE-ICs into the SCS where they were captured and disaggregated before being

conveyed along macrophage cell processes from the lumen into the follicle (Supplementary Movie 1 and Fig. 2f). Rare CFP+ B cells could be observed moving within the follicle as expected and, in one instance, a B cell was seen migrating briefly on the sinus-facing side of a macrophage. Analysis of high-resolution images (0.6 μm/pixel) from multiple individual 'confocal' *z* stacks showed that the discrete PE-ICs appeared to move along the surface membrane of SCS macrophages as defined by CD169 labeling. Furthermore, on the occasions where individual cell bodies were clearly defined, the PE-ICs were rarely observed to be internalized or to travel within the body of the cell. Thus SCS macrophages capture ICs and appear to retain them on their surface for rapid translocation into the follicle along cellular processes.

SCS macrophages have low levels of lysosomal enzymes

To investigate the poorly endocytic, poorly degradative nature of SCS macrophages we asked if they differentially expressed genes associated with lysosomal degradation. Cells were enriched ~5–10-fold from protease-digested peripheral lymph nodes of wild-type mice by Percoll density gradient separation and then sorted by flow cytometry into DAPI$^-$ B220$^-$ CD4$^-$ CD8$^-$ CD169^{hi} CD11c^{lo} CD11b$^+$ F4/80$^-$ SCS and DAPI$^-$ B220$^-$ CD4$^-$ CD8$^-$ CD169^{hi} CD11c^{lo} CD11b$^+$ F4/80$^+$ medullary macrophages with ~95% purity (Fig. 3a). By gene expression analysis, sorted SCS and medullary macrophages showed abundant and similar expression of housekeeping genes (Fig. 3b) and a large array of macrophage transcription factors (Fig. 3c), confirming that both cell types are of the macrophage lineage. Q-PCR analysis confirmed that *Sfpi1* transcripts that encode the macrophage- and B cell-specific transcription factor PU.1, were highly expressed (Fig. 3d). However, SCS macrophages had reduced transcript abundance for lysosome-associated membrane proteins–1 and –2, lysozyme, a panel of lysosomal proteases and vacuolar ATPases required to acidify the lysosome (Fig. 3e). Immunofluorescence microscopy of the isolated cells showed the SCS macrophages were smaller and had markedly reduced LAMP-1 staining compared to medullary macrophages (Fig. 3f). Intracellular flow cytometry analysis revealed approximately one-fifth the abundance of LAMP-protein expression in the SCS macrophages (Fig. 3g). These data suggest that SCS macrophages are poorly degradative because of low expression of lysosomal proteins.

SCS macrophages require B cell-derived lymphotoxin

The distribution of SCS macrophages was closely coordinated with the distribution of B cells (Fig. 1a), suggesting a morphogenic interplay. Examination of B cell-deficient mice revealed one-tenth the number of SCS macrophages in their inguinal lymph nodes compared to wild-type controls (Fig. 4a–c). The macrophages remaining were enriched for cells with an F4/80$^+$ medullary phenotype (Fig. 4a,b). B cells are a known source of lymphotoxin (LT)-$\alpha_1\beta_2$, a heterotrimeric cytokine that influences macrophage populations in the spleen14, 15. Whereas transfers of wild-type B cells to B cell-deficient mice could partially restore the SCS macrophage compartment, LTα-deficient B cells were unable to increase the numbers of these cells (Fig. 4c). Transgenic overexpression of LT$\alpha_1\beta_2$ selectively in B cells16 led to a 2–3 fold increase in total SCS macrophage numbers without affecting B cell numbers (Fig. 4d) and a thicker layer of SCS macrophages overlying the B cell areas (Fig. 4e). SCS and medullary macrophages both expressed transcripts for the lymphotoxin

receptor LTβR (Fig. 4f) and showed LTβR surface staining by flow cytometery (Fig. 4g). In mixed radiation chimeras reconstituted with *Ltbr*$^{-/-}$ and wild-type bone marrow, there was a selective deficiency in *Ltbr*$^{-/-}$ SCS macrophages establishing an intrinsic requirement for the receptor in these cells or their precursors (Fig. 4h). The requirement for LTβR signaling appeared constitutive as LTβR-Fc treatment for 4 weeks led to an almost complete ablation of this cell population while having a milder effect on medullary macrophage numbers (Fig. 4i,j). This SCS macrophage ablation in turn led to a severe defect in the ability of follicular B cells to capture PE-ICs, assessed by examining PE mean fluorescence intensity of draining lymph node B cells isolated 2 h after PE injection (Fig. 4k). The PE mean fluorescence intensity of Ly5.2^{+} B cells added at the time of lymph node cell isolation provides a measure of the 'non-specific' *in vitro* capture of PE-ICs (Fig. 4k). Furthermore, short term LTβR blockade for 3 days had little effect on total SCS macrophage cell numbers but did affect their function in PE-IC capture (Fig. 4l, left panel) and caused a reduction in delivery of PE-IC to follicular B cells (Fig. 4l, right panel). Thus, constitutive lymphotoxin signals provided by B cells are important for SCS macrophage development and their efficient relay of ICs to follicular B cells.

Non-cognate B cells relay ICs into the GC

Antigen capture and follicular relay by SCS macrophages is likely to be most active when preformed IgG antibody is available. This notion led us to ask whether the relay of ICs by this pathway was important during the GC response. To show that newly generated antibodies can feedback to opsonize antigen and form ICs for delivery into GCs, we adoptively transferred avian lysozyme-specific Hy10 B cells and ovalbumin (OVA)-specific OT-II T cells and immunized recipient mice with duck egg lyzosyme (DEL) conjugated to OVA to provide linked T cell help11. Hy10 B cells recognize DEL with low affinity and hen egg lysozyme (HEL) with high affinity. Seven days after primary challenge with DEL-OVA, recipient mice were rechallenged with additional cognate antigen HEL-PE or non-cognate nitrophenol (NP)-PE as a control. 8 h after rechallenge we observed deposition of antigen-specific ICs containing HEL-PE but not NP-PE in GCs (Fig. 5a). In reciprocal experiments, we transferred 'quasi-monoclonal' QM B cells specific for the hapten NP (ref 17) and immunized recipient mice with NP-chicken gamma globulin, NP-CGG (Fig. 5b). On day 7 we rechallenged recipient mice with HEL-PE or NP-PE and observed deposition of NP-PE containing ICs but not HEL-PE-ICs. These results indicate that newly generated antibodies opsonize incoming antigen for delivery to GCs and deposition on FDCs.

We next asked if we could directly visualize transport of opsonized antigen into the GC by non-cognate B cells. To perform tracking studies of cells by real-time two photon microscopy, only a few percent of the total cells can be labeled18. Hy10 B cells expressing green fluorescent protein (GFP) and OT-II T-cells were adoptively transferred into either wild-type or *Cr2*$^{-/-}$ BM chimeras (lacking CR1 and CR2 on endogenous hematopoietic cells but retaining these molecules on radiation resistant FDCs) and the mice were immunized with DEL-OVA to promote lysozyme-specific antibody production and initiate GC formation. We then transferred wild-type polyclonal CFP-transgenic B cells into the mice on day 6. On day 7 HEL-PE was injected subcutaneously to generate red fluorescent antigen-containing ICs and explanted lymph nodes were imaged 3 h later (Supplementary Movies 2–

4 online). At this time point, all detectable GFP$^+$ cells correspond to GC B cells11. *Cr2*$^{-/-}$ BM chimeras were used as recipients in some experiments in an effort to improve the chances that imaged CFP-transgenic B cells would be IC bearing, though similar findings were obtained in *Cr2*$^{-/-}$ (Supplementary Movie 2 and 4) and wild-type (Supplementary Movie 3) recipients. These two-photon microscopy experiments showed CFP$^+$ non-cognate B cells loaded with HEL-PE in their trailing uropod migrating from the subcapsular region through the follicular mantle zone into the GFP$^+$ GC light zone (Supplementary Movies 2,3 and Fig. 5c). CFP$^+$ B cells laden with HEL-PE could also be observed migrating deep within the GC light zone (Supplementary Movie 4). This antigen transport into GCs was CR1/2-dependent as delivery of opsonized antigen into GCs was impaired in *Cr2*$^{-/-}$ chimeras that did not contain wild-type polyclonal B cells (Fig. 5d). Thus follicular B cells deliver endogenously formed ICs into GCs in a CR1/2-dependent manner.

IC relay drives antibody affinity maturation

Finally, we asked if IC relay from SCS macrophages to B cells to the GC played any role in the GC response and affinity maturation. In initial experiments we noted that single gene deficiencies in *Itgb2* (encoding the integrin β2 chain that is part of CR3), *Itgam* (encoding the α chain of CR3) or *Fcgr2b* (encoding FcγRIIb) had limited effects on the IC relay, suggesting redundant mechanisms of IC capture by SCS macrophages. These gene deficiencies therefore did not allow us to clearly assess the functional consequences of perturbations in the pathway. Moreover, attempts at genetic and pharmacological ablation of SCS macrophages either led to altered inflammatory conditions or affected other cell types such as FDCs that themselves impacted the GC response (data not shown). We therefore turned to an alternative approach of testing the importance of the IC relay and examined the impact of disrupting the ability of non-cognate B cells to function as antigen transport cells by removing complement receptors from these cells. Since CR1/2 also has a role on FDC and as a co-receptor on cognate B cells19 we used the same adoptive transfer system as above where the FDC and cognate B cells were CR1/2 wild-type but the non-cognate follicular B cells were either CR1/2-deficient or wild-type (Supplementary Fig. 2 online). Thus, CR1/2-deficient or control BM chimeras received adoptive transfer of small numbers of wild-type antigen-specific Hy10 B cells and OT-II T-cells and were then immunized with DEL-OVA in a depot-forming adjuvant and the GC response mounted by the CR1/2-sufficient Hy10 B cells was examined. At day 7, prior to affinity maturation, the magnitude of the GC and antibody response was equivalent in the two groups, suggesting that cognate B cells were able to directly access antigen from SCS macrophages or other sources and initiate the response (Supplementary Fig. 2). However, at day 14 the magnitude of the GC response in mice lacking IC transport-competent B cells was approximately half that of wild-type B cell-reconstituted mice (Fig. 6a,b). Importantly, while class switching occurred normally, there was less affinity maturation as assessed by flow cytometry for GC B cell binding of the low-affinity antigen (Fig. 6a,b) and serum antibody binding in ELISA assays (Fig. 6c). Thus, while serum anti-HEL Igκ titers were similarly increased from day 7 to day 14, there was a less marked rise in high affinity anti-DEL Igκ antibodies in *Cr2*$^{-/-}$ BM chimera recipients than wild-type chimeras (Fig. 6c). To directly show there was a difference in affinity based selection, we sorted single cells by flow cytometry from recipient mice on day 14 of the response and PCR-amplified and analysed the *Igh* variable

region gene for somatic hypermutation (Fig. 6d). Sequence analysis showed significantly more enrichment of Hy10 B cells with the canonical high-affinity Y53F mutation11 in wild-type (34 of 46 sequences) than *Cr2*$^{-/-}$ BM chimeras (23 of 53; $P = 0.002$, Fischer's exact test). Although disruption of IC relay affected the GC B cell response there was no significant difference in the number of OT-II Tcells recovered (Supplementary Fig. 2). These data indicate that follicular B cells transport opsonized antigen into GC light zones to enhance the GC response and affinity maturation is blunted when this IC relay pathway is disrupted.

Discussion

The above findings demonstrate that SCS macrophages are a unique poorly endocytic macrophage cell type with low degradative capacity. These LT$\alpha_1\beta_2$-dependent cells deliver intact antigen-containing ICs captured in the SCS along membrane processes into the follicle. Newly generated ICs are delivered to the GC light zone in a CR1/2-dependent manner by antigen-transporting B cells, a process that influences the magnitude and quality of the GC response. Together these findings suggest that the relay of ICs from SCS macrophages to follicular B cells and then to light zone FDCs and GC B cells helps drive antibody affinity maturation by mediating the ongoing GC delivery of antigen and competing antibody.

Early electron microscopy studies of horseradish peroxidase-containing ICs deposited on cells in the SCS floor suggested they were sequestered on the cell surface or in plasma membrane infoldings3. More recently, electron microscopy of captured vesicular stomatitis virus showed virions on the cell surface but also in vacuoles6. Two-photon microscopy revealed that B cells could capture antigens and ICs from SCS macrophages further establishing that these cells are able to display antigens on their cell surface4–6. Our analysis here of isolated cells demonstrates that SCS macrophages retain a greater proportion of the ICs they capture on their surface than the nearby medullary macrophages. Moreover, our data show that these cells have reduced lysosomal function, a property that may facilitate recycling of internalized antigen back to the cell surface. As well as being necessary for their antigen presentation function, the reduced degradative capacity of SCS macrophages might make them a 'safe-haven' for some intracellular pathogens20.

Ultrastructural studies and intravital two-photon microscopy showed that macrophage processes ('heads') protruded into the SCS and were positioned in the lymph flow to capture ICs as they drained from the afferent lymphatic vessel2–6, 21. By tracking the behavior of captured complexes on SCS macrophage 'tail' processes, we found that ICs fragmented as they were moved along the process, perhaps the effect of forces exerted on the complexes as they passed the junction between the SCS macrophage and the sinus lining cells they insert themselves through3. The basis for the unidirectional movement of particles along the macrophage surface is not yet clear but in preliminary analysis we find that the macrophages have a polarized distribution of transmembrane proteins (T.G.P., E.E.G. and J.G.C., unpublished observations) suggesting they are organized to mediate directional membrane transport. Anterograde membrane flow is a common feature of polarized migrating cells and is sufficient to move a variety of particle types over the membrane surface in an actin-

dependent manner22. T cells polarizing towards a target cell show directed movement of membrane over their surface to the site of synapse23, 24. It seems possible that a related form of surface molecule treadmilling could occur to promote unidirectional movement of IC binding proteins in SCS macrophages. Alternatively, perhaps there is sufficient lymph flow over the surface of SCS macrophages to provide shear forces that mediate directional movement of surface molecules. Shear forces exerted by hydrodynamic flow cause 'sailing' of ICs on the trypanosome membrane surface25. Finally, the possibility that ICs are transported inside the cell in a specialized form of transcytosis is not yet excluded. Future studies will need to characterize the membrane polarity of SCS macrophages and determine the molecular requirements for SCS to follicular movement of ICs.

B cell-derived $LT\alpha_1\beta_2$ has an established role in promoting FDC development in lymphoid tissues14. $LT\alpha_1\beta_2$ is also required for maintenance of marginal zone macrophage populations in the spleen14 and for homeostasis of splenic DCs26. The dependence of lymph node SCS macrophages on $LT\alpha_1\beta_2$ suggests disruption in antigen-relay, as well as the loss of FDCs, contributes to the reduced antibody responses observed in LTα-deficient mice14, 15. The impact of depleting these cells should be considered during the ongoing clinical trials of $LT\alpha_1\beta_2$ antagonism in humans15. The role of B cells as a key source of $LT\alpha_1\beta_2$ for SCS macrophage development or maintenance indicates that B cell follicles help themselves acquire a uniform coverage of SCS macrophages. This interplay likely ensures that as a lymph node enlarges in response to immunization or infection, and the B cell representation increases due to recruitment, retention and proliferation, the overlying SCS macrophage population increases concordantly.

The demonstration that CR1/2 on non-cognate follicular B cells is important for IC delivery to the GC establishes a third site where CR1/2 acts during the antibody response, a finding that may resolve some of the discrepancies in earlier investigations examining the role of CR1/2 on FDCs or cognate B cells19. The importance of follicular B cells in mediating antigen delivery to the GC is consistent with the recent demonstration that follicular B cells gain access to the GC light zone10, 11. As well as delivering ICs to FDCs, IC-laden follicular B cells appear likely to play a direct role in presentation as they travel through the GC. Antigen encounter by B-B cellular interactions might help explain how in some studies, GC formation and somatic hypermutation could take place in the apparent absence of IC-capturing FDCs27, 28. Although it has long been suggested that the early antibody response plays an important role in the later GC response, this has largely been studied by testing the effects of exogenously administered antibody on the endogenous response29–31. An exception is the finding that mice with targeted disruption of the IgM secretory region that lack secreted IgM have a reduced GC response and delayed affinity maturation32, 33. Whether this reflected a role of natural antibody or newly produced antibody was unclear. The macrophage-B cell IC relay that we describe may principally have arisen to mediate efficient delivery of even minute amounts of antigen, as well as antibody, to the GC to help drive on-going affinity maturation. Approaches to target antigens to SCS macrophages and that thus facilitate delivery to GCs might allow improved vaccine design.

Methods

Mice

6–12 week old wild-type and Ly5.2 (CD45.1) congenic mice C57BL/6 (B6) were from either National Cancer Institute or Jackson Laboratories. B6 mice expressing CFP under the β-actin promoter34 (004218; Tg(ACTB-ECFP)1Nagy/J), mice expressing GFP under the human ubiquitin promoter35 (004353; Tg(UBC-GFP)30Scha/J) and B cell-deficient *Igh-6*$^{-/-}$ mice36 (002288; B6.129S2-*Igh-6*^{tm1Cgn}/J), were from Jackson Laboratories. Mice deficient for LTα37 (B6.129S2-*Lta*^{tm1DCh}) and LTβR38 and mice overexpressing membrane-bound LTα under the Igκ promoter (line b10) have been described16 and were ten or more generations backcrossed to B6. Homozgyous six month-old κLTα transgenic mice and age-matched controls were analyzed. *Cr2*$^{-/-}$ deficient for both CR1 and CR2 (ref. 39), Hy10 mice (previously named VDJ9/κ5 mice) expressing a knock-in BCR with high affinity for hen egg lysosome (HEL) and low affinity for duck egg lysozyme (DEL)11 and OT-II TCR transgenic mice40 were all 10 or more generations backcrossed to B6. Hy10 mice homozygous for the ubiquitin GFP-transgene were used for imaging studies. QM mice expressing knock-in BCR specific for NP were as described17. Animals were housed in a germ-free environment in the Laboratory Animal Research Center at UCSF and all experiments conformed to the ethical principles and guidelines approved by the UCSF Institutional and Animal Care and Use Committee.

Bone marrow chimeras and adoptive transfers

Ly5.2 congenic mice were lethally irradiated with either 1100 or 1300 rads in split doses and reconstituted with 1–3 × 10^6 bone marrow cells from wild-type and *Cr2*$^{-/-}$ donors. Mixed bone marrow chimeras were made with a 80:20 mix of *Ltbr*$^{-/-}$:Ly5.2 bone marrow into wild-type (Ly5.1) recipients. Mice were analyzed 8–12 weeks later. For B cell reconstitution experiments, B cells were negatively isolated from wild-type or *Lta*$^{-/-}$ mice using the AutoMACS cell separator (Miltenyi) and biotinylated antibodies to CD11c clone HL3 and CD43 clone S7 (both from BD Pharmingen) and MACS streptavidin microbeads (Miltenyi) as described5. 2–3 × 10^7 B cells were transferred into *Igh-6*$^{-/-}$ mice and recipient mice were analysed 14 days later. B cells were typically >95% pure as assessed by flow cytometric analysis on a FACSCalibur. Transferred B cells typically reconstituted 2–8% of lymph node cells.

In vivo immune complex generation and endocytosis

PE-ICs were generated as described5. To generate BSA-anti-BSA ICs, polyclonal rabbit IgG anti-BSA antibodies (Invitrogen) were dialyzed and conjugated to Alexa Fluor 647 (Molecular Probes). Mice were given 2 mg i.p. of the labeled antibody 12–16 h before s.c. injection of 20 μg of DQ Green BSA (Invitrogen) per draining lymph node. For analysis, cells were isolated from draining lymph nodes together with lymph nodes from a Ly5.2 congenic mouse that did not receive ICs as describe5.

Tissue digestion and flow cytometry

Lymph nodes were carefully dissected free of fat and fascia and gently teased apart with microforceps into DMEM containing penicillin/streptomycin and HEPES buffer pH 7.2. The tissue was then digested with Liberase Blendzyme 2 (Roche Applied Science) at 0.2 mg/ml and DNAse I at 20 μg/ml for 20–30 min. Proteases were then inactivated with 10% fetal bovine serum (FBS) and 5 μM EDTA (unless ICs were present) and disaggregated by passing through a 100 μm nylon sieve (BD Bioscience). Single cells were then washed, blocked with 2.4G2 (UCSF Hybridoma Core Facility) and 5% normal mouse and normal rat serum and stained for flow cytometric analysis as described5. For identifying SCS macrophages Ser-4 mAbs against CD16941 were purified from ascites fluid and conjugated to either Alexa Fluor 488 or Alexa Fluor 647 using the antibody labeling kits from Molecular Probes. Antibodies used included those against B220-PE or -PerCp clone RA3-6B2 (BD Pharmingen), CD4-PerCp clone RM4-5 (BD Pharmingen), CD8α-PerCp clone 53–6.7 (BD Pharmingen), CD11b-FITC or -PE clone Mac-1 (Invitrogen), CD11c-FITC or -PE clone HL3 (BD Pharmingen), CD45.1-Pacific Blue clone A20 (Biolegend), CD45.2-A700 or -Pacific Blue clone 104 (both from Biolegend), F4/80-biotin (Cedarlane Laboratories) or –Alexa Fluor 647 clone Cl:A3-1 (Biolegend) and streptavidin-Qdot 605 (Molecular Probes). DEL was purified as described11. For analysis of B cell responses HEL (Sigma) and DEL were directly conjugated to Alexa Fluor 647 and conjugated antigen isolated using Bio-Spin 6 columns (Bio-Rad). GC cells were identified with antibodies to IgD-FITC clone 11-26c.2a (BD Pharmingen), Fas-PE clone Jo2 (BD Pharmingen), and IgG_{2b}-biotin clone RMG2b-1 (Biolegend). HEL-Alexa Fluor 647 was used to detect HEL-specific B cells and DEL-Alexa Fluor 647 used to detect somatically mutated cells that had acquired high affinity for the original antigen11. Plasma cells were identified by intracellular staining as described42. Briefly, cells were fixed for 20 min in 2% paraformaldehyde and then permeabilized overnight with 0.2% polyethylene sorbitan monolaurate before washing and staining with HEL-Alexa Fluor 647 and antibodies to syndecan-1-biotin clone 281-2 (BD Pharmingen), B220-PE and CD45.1-FITC (BD Pharmingen). Intracellular staining for LAMP-1 and LAMP-2 was performed with anti-LAMP-1-FITC clone 1D4B and anti-LAMP-2-FITC clone ABL-93, respectively. Staining for surface expression of LTβR was performed using purified hamster mAb AF:H6 and detected with anti-Armenian and Syrian hamster IgG cocktail conjugated to PE (BD Pharmingen) as described26. Data was acquired on an LSRII and analysed using FlowJo software (Treestar Inc.).

Stripping of surface-bound ICs

In acid stripping experiments, mice were administered PE-ICs and 4 h later lymph node cells were washed in PBS at 4°C before exposure to 0.5 M NaCl/0.2 M acetic acid for 4 min at 4°C 43. Cells were then washed three times before staining.

Macrophage isolation and cell sorting

For cell sorting, lymph node cells prepared as above were resuspended in DMEM, 2% FBS, 5 μM EDTA and loaded onto an ice-cold density gradient layered with 50% and 30% Percoll (Amersham). The column was spun at 365 × *g* for 25 min with no brakes. Cells at the 50%/30% interface contained large cells that were typically enriched 10-fold for CD169-

expressing cells. Fc receptors were then blocked with 2.4G2 in 5% normal rat serum and 5% normal mouse serum before staining in DMEM, 2% FBS, 5 μM EDTA with CD11c-FITC, CD11b-PE, B220-, CD4- and CD8-PerCp, CD169-Alexa Fluor 647, F4/80-biotin and streptavidin-Qdot 605. Live single cells that excluded DAPI (Molecular Probes) were gated and sorted for $CD11c^{int}$ $CD11b^{+}$ $B220^{-}CD4^{-}CD8^{-}CD169^{hi}$ $F4/80^{-}$ (SCS macrophages) and $CD11c^{int}$ $CD11b^{+}$ $B220^{-}CD4^{-}CD8^{-}CD169^{hi}$ $F4/80^{+}$ (medullary macrophages) subsets on a FACSAria. Cells were typically ~95% pure when re-analyzed for cell sorting parameters.

Gene expression profiling and real-time PCR

The data discussed in this publication have been deposited in NCBI's Gene Expression Omnibus and are accessible through GEO Series accession number GSE15767 (http://www.ncbi.nlm.nih.gov/geo/query/acc.cgi?acc=GSE15767). Total RNA was isolated from ~20,000 sorted SCS and medullary macrophages with the RNEasy Micro Kit (Qiagen). RNA was amplified using the Ovation RNA Amplification System V2 and amplified cDNA fragmented and labeled with FL-Ovation cDNA Biotin Module V2 (both from NuGen). Samples from 3 independent experiments were then hybridized to Affymetrix Genechip array, stained, scanned and normalized by the UCSF Gladstone Genomics Core facility. Normalized data was analyzed using Remote Analysis Computation for gene Expression data (http://race.unil.ch/). Housekeeping genes used to validate the microarray were from44. The list of macrophage transcription factors used to establish the haematopoietic cell lineage of sorted cells was from45. Gene expression profiles depicted in Figure 3b,c and e were defined as those with probe signals $>2^{6}$ and a Baynesian false discovery rate <0.05. For quantitative RT-PCR, non-amplified cDNA was reacted with primer-probe sets (Integrated DNA Technologies) and SYBR Green PCR Master Mix (Applied Biosystems) on a 7300 Real-Time PCR System (Applied Biosystems). The relative mRNA abundance of target genes was determined by subtracting the threshold cycle for the housekeeping gene *(Hprt1)* from the target gene.

Adoptive transfers and immunizations

T-dependent immune response was tracked using Hy10 B cells as previously described11. Briefly, IgM^{a}-expressing HEL-specific B cells were negatively isolated from Hy10 mice by AutoMACS depleting cells labeled with biotinylated antibodies to CD11c, CD43, Ly6C (BD Pharmingen), IgM^{b} clone AF6-78 and IgD^{b} clone 217-170 (both from BD Pharmingen) and MACS streptavidin microbeads. Frequency of HEL-specific B cells was typically ~70% as assessed by flow cytometric staining for IgM^{a} clone DS-1 (BD Pharmingen) and HEL-binding. OVA-specific T cells were negatively isolated from OT-II mice by AutoMACS depleting cells labeled with biotinylated antibodies to B220 clone RA3-6B2 (BD Pharmingen), CD11b clone Mac-1 (CALTAG), CD11c and Ly6C clone AL-21 and MACS streptavidin microbeads. Frequency of OVA-specific T cells was typically ~70% as assessed by flow cytometry for $V_{\alpha}2$-FITC clone B20.1and $V_{\beta}5$-PE clone MR9-4 (both from BD Pharmingen). 10^{5} HEL-specific B cells and OVA-specific T cells were then adoptively transferred into wild-type or $Cr2^{-/-}$ BM chimeras. Mice were then challenged with 10 μg of DEL-OVA in Sigma Adjuvant System (Sigma) in both lateral chest walls below the scapula (to drain the brachial lymph nodes) and both flanks and 5 μg in both tail base (to drain the inguinal lymph nodes). Seven or 14 days later serum was collected for ELISA and lymph

nodes harvested for flow cytometry analysis and histology. For assessment of antigen transport into the GC, Hy10 B cells and OT-II T cells were adoptively transferred into Ly5.1 congenic recipients and immunized with DEL-OVA as above. On day 7 mice were given additional specific antigen HEL-PE or non-specific NP-PE. 8 h later draining lymph nodes were harvested for immunofluorescence microscopy. Reciprocally, QM B cells specific for NP were adoptively transferred and immunized with NP-CGG. On day 7 mice were re-challenged with either HEL-PE or NP-PE and analyzed for deposition of opsonized antigen in GCs 8 h later. To test the requirements for B cell antigen transport, wild-type or *Cr2*$^{-/-}$ BM chimera recipients were re-challenged on day 7 with HEL-OVA and lymph nodes harvested 8 h later for immunohistochemistry. For two-photon microscopy, 9.5×10^4 Hy10 B cells and 5×10^3 Hy10 B cells expressing GFP were transferred together with 10^5 OT-II T-cells and challenged them with DEL-OVA in adjuvant. On day 7, mice were re-challenged s.c. with 10 μg HEL-PE and 3-4 h later draining lymph nodes harvested. HEL-PE was produced by incubating HEL-biotin in molar excess with streptavidin-PE and removing unbound HEL-biotin using the Bio-Spin 30 column (Bio-Rad).

ELISA

ELISA was performed as previously described46. Briefly, 96-well polystyrene plates (Nunc) were coated with 10 μg/ml of either HEL or DEL at 4 °C overnight and then blocked with 5% skim milk powder in PBS. Sera in 0.1% BSA in PBS was then serially diluted in duplicates together with HyHEL9 and HyHEL10 mAb as positive control for anti-HEL ELISA. For anti-DEL ELISA, the HyHEL10 mAb (which has the same specificity as the Hy10 knock-in BCR) did not react with DEL and served as a negative control and HyHEL9 mAb which recognized a different epitope47 served as a positive control. Bound antibodies were detected with biotinylated anti-Igκ clone 187.1 (BD Pharmingen) in 0.1% BSA, 1% skim milk in PBS. Streptavidin-AP (Jackson Immunoresearch) was visualized with the substrate *p*-nitrophenyl phosphate (Fisher) and the absorbance read at 405 nm on a SpectraMax spectrophotometer (Molecular Devices). A standard curve was constructed for the HyHEL9 mAb and used to determine the equivalent amounts of HEL- and DEL-specific Igκ antibodies.

Light and fluorescent microscopy

Sorted SCS and medullary macrophages were resuspended at 10^7 cells/ml in 10% FBS in RPMI and incubated on glass coverslips (Fischer) at 37°C for >4 h. Adherent cells were fixed for 20 min with 2% paraformaldehyde and then permeabilized with 0.05% Triton X-100 before washing and restaining with CD169-Alexa Fluor 647, anti-LAMP-1-PE clone 1D4B (BD Pharmingen) and DAPI. The coverslip was then mounted on a glass slide with Fluoromount-G (Southern Biotechnology) and DIC and fluorescent images obtained with a Zeiss AxioObserver Z1 inverted microscope.

Immunohistochemistry was performed as described11. Briefly, 7 μm thick lymph node sections were fixed in acetone and rehydrated with 0.1% BSA/TBS and blocked with 2% normal mouse serum, 0.1% BSA in TBS. Slides were washed and stained with anti-CD169 mAb detected with donkey anti-rat IgG (H+L)-HRP (Jackson Immunoresearch) blocked with 5% normal rat serum and stained with B220-biotin detected with streptavidin-AP.

HEL-binding plasma cells were identified by staining sections with HEL at 200 ng/ml followed by rabbit polyclonal IgG anti-HEL-biotin (Rockland) and detected with streptavidin-AP. GCs were identified as IgD negative areas within the follicle by staining with IgD-FITC and detected with anti-FITC-HRP (Roche Applied Science).

Immunofluorescence microscopy was performed as described5. Acetone-fixed 5 μm sections were stained with anti-CD169-Alexa Fluor 488, anti-F4/80-biotin and streptavidin-PE and B220-APC clone RA3-6B2 (BD Pharmingen). Tiled images were captured and assembled on a Zeiss AxioObserver Z1. For confocal microscopy, 10–30 μm sections were stained with Ser4-Alexa Fluor 488, anti-F4/80-biotin and streptavidin-PE (BD Pharmingen) and B220-APC clone RA3-6B2 (BD Pharmingen) and images captured on a Leica TCS SL confocal microscope using the 488, 543 and 633 nm laser lines to excite Alexa Fluor 488, PE and Alexa Fluor 647, respectively. Emission slits were tuned to 498–540 nm for FITC, 560–600 nm for PE and 643–710nm for Alexa Fluor 647. Confocal images were processed using Adobe PhotoShop CS2.

Intravital microscopy and two-photon imaging

Intravital microscopy was performed essentially as described5. Mice were injected s.c. in the left flank and tail base with 20 μg of anti-CD169-Alexa Fluor 488 to label the SCS macrophages *in vivo* 12–16 h before imaging. For anaesthesia, mice were injected with 500 μl i.p. of anaesthetic solution (ketamine 5mg/ml and xylazine 1mg/ml) and deep anaesthesia maintained with 100–200 μl injected every 20–30 min as needed into the tail base contralateral to the imaging side. Anaesthetised mice were given supplementary oxygen via a nose cone and positioned on a Biotherm Micro S37 stage warmer maintained at 37 °C. To image the inguinal lymph node a skin flap was mobilized by blunt dissection and glued to a silicone base with Vetbond (3M). A window was made in the overlying skin and fat, connective tissue and fascia was carefully microdissected to reveal the cortical surface of the node. The node was then perfused with warm RPMI diffused with 5% CO_2:95% O_2 and imaged through the intact capsule. The temperature inside the meniscus was monitored and maintained at 35.8–37.5 °C with a single inline solution heater coupled to a temperature controller (Warner Instruments). To image the GC, HEL-specific Hy10 B cells expressing GFP were transferred into *Cr2*$^{-/-}$ BM chimeras and challenged with DEL-OVA in adjuvant as above. The day before imaging, 1–3 × 10^7 CFP expressing B cells were transferred to delineate the follicular mantle zone. On day 7, mice were re-challenged s.c. with 10 μg HEL-PE and 3–4 h later draining lymph nodes harvested and explanted lymph nodes were prepared for two-photon imaging as described48. Deep tissue images were acquired with a custom-built two-photon microscope (M. Krummel, UCSF). A MaiTai TiSapphire laser (Spectra-Physics) was tuned to provide an excitation wavelength of 910 nm. Each *xy* plane spanned 480 × 400 pixels at a 0.6 μm/pixel resolution and 40–50 *xy* planes with 2–3 μm *z* spacings were formed by averaging 10 video frames every 20–30 s. Emission wavelengths used were 440–500 nm (CFP and second harmonic emission of collagen fibers), 500–550 nm (GFP and Alexa Fluor 488) and 567–640nm (PE-ICs and HEL-PE-ICs). Images were acquired with Video Savant (IO Industries) and maximum intensity time-lapse images generated with MetaMorph (Molecular Devices). Videos were processed with a median noise filter. Cell tracks and 3D rotation images were made with Imaris 5.01 × 64 (Bitplane)

and images filtered with a median filter. Annotation and final movie compilation was performed in Adobe After Effects 7.0. Video files were converted to mpeg format with Avi to Mpeg Converter for Windows 1.5 (FlyDragon Software).

Single cell PCR and SHM analysis

For analysis of mutated sequences, single donor-derived GC B cells specific for HEL on day 14 of the response were sorted into 96-well plates and their *Igh* variable genes sequenced as described11.

Statistical analysis

All statistical analysis was performed in GraphPad Prism (GraphPad Software). Means between two groups were compared using one-tailed t test. For analysis of SHM data in Fig. 6d we constructed a 2 × 2 contingency table and performed a Fischer's exact test.

Supplementary Material

Refer to Web version on PubMed Central for supplementary material.

Acknowledgments

We thank L. Shiow for cell sorting and helpful discussions, K. Suzuki for preparation of HEL-PE, C. Allen for help with single cell sorting, I. Girgorova for help with video editing, J. An for mouse screening, J. Atkinson (Washington University) for CR2-deficient mice, M. Wabl for QM mice, J. Browning (Biogen Idec) for LTβR-Fc, P. Crocker (University of Glasgow) for Ser-4 antibody, A. Bullen and M. Krummel for help with the two-photon microscope, and A. Bankovich for helpful advice. We also thank the UCSF Hybridoma Core, Gladstone Genomics Core, DERC Microscopy Core and Biological Imaging Development Center. T.G.P. is an National Health and Medical Research Council CJ Martin fellow, J.G. is National Science Foundation Graduate Research fellow and J.G.C. is an Investigator of the Howard Hughes Medical Institute. This work was supported by NIH grants AI45073 and AI40098 and by a Sandler New Technology Award.

References

1. Nossal GJ, Abbot A, Mitchell J, Lummus Z. Antigens in immunity. XV. Ultrastructural features of antigen capture in primary and secondary lymphoid follicles. J. Exp. Med. 1968; 127:277–290. [PubMed: 4169585]
2. Fossum S. The architecture of rat lymph nodes. IV. Distribution of ferritin and colloidal carbon in the draining lymph nodes after foot-pad injection. Scand. J. Immunol. 1980; 12:433–441. [PubMed: 7466330]
3. Szakal AK, Holmes KL, Tew JG. Transport of immune complexes from the subcapsular sinus to lymph node follicles on the surface of nonphagocytic cells, including cells with dendritic morphology. J. Immunol. 1983; 131:1714–1727. [PubMed: 6619542]
4. Carrasco YR, Batista FD. B cells acquire particulate antigen in a macrophage-rich area at the boundary between the follicle and the subcapsular sinus of the lymph node. Immunity. 2007; 27:160–171. [PubMed: 17658276]
5. Phan TG, Grigorova I, Okada T, Cyster JG. Subcapsular encounter and complement-dependent transport of immune complexes by lymph node B cells. Nat. Immunol. 2007; 8:992–1000. [PubMed: 17660822]
6. Junt T, et al. Subcapsular sinus macrophages in lymph nodes clear lymph-borne viruses and present them to antiviral B cells. Nature. 2007; 450:110–114. [PubMed: 17934446]
7. Steinman RM, Banchereau J. Taking dendritic cells into medicine. Nature. 2007; 449:419–426. [PubMed: 17898760]
8. MacLennan ICM. Germinal Centers. Annu. Rev. Immunol. 1994; 12:117–139. [PubMed: 8011279]

9. Allen CD, Okada T, Cyster JG. Germinal-center organization and cellular dynamics. Immunity. 2007; 27:190–202. [PubMed: 17723214]
10. Schwickert TA, et al. In vivo imaging of germinal centres reveals a dynamic open structure. Nature. 2007; 446:83–87. [PubMed: 17268470]
11. Allen CD, Okada T, Tang HL, Cyster JG. Imaging of germinal center selection events during affinity maturation. Science. 2007; 315:528–531. [PubMed: 17185562]
12. Crocker PR, Gordon S. Properties and distribution of a lectin-like hemagglutinin differentially expressed by murine stromal tissue macrophages. J. Exp. Med. 1986; 164:1862–1875. [PubMed: 3783087]
13. Hume DA, Robinson AP, MacPherson GG, Gordon S. The mononuclear phagocyte system of the mouse defined by immunohistochemical localization of antigen F4/80. Relationship between macrophages, Langerhans cells, reticular cells, and dendritic cells in lymphoid and hematopoietic organs. J. Exp. Med. 1983; 158:1522–1536. [PubMed: 6355361]
14. Fu Y-X, Chaplin DD. Development and maturation of secondary lymphoid tissues. Ann. Rev. Immunol. 1999; 17:399–433. [PubMed: 10358764]
15. Browning JL. Inhibition of the lymphotoxin pathway as a therapy for autoimmune disease. Immunol. Rev. 2008; 223:202–220. [PubMed: 18613838]
16. Ngo VN, Cornall RJ, Cyster JG, Splenic T. zone development is B cell dependent. J. Exp. Med. 2001; 194:1649–1660. [PubMed: 11733579]
17. Cascalho M, Ma A, Lee S, Masat L, Wabl M. A quasi-monoclonal mouse. Science. 1996; 272:1649–1652. [PubMed: 8658139]
18. Germain RN, Miller MJ, Dustin ML, Nussenzweig MC. Dynamic imaging of the immune system: progress, pitfalls and promise. Nat. Rev. Immunol. 2006; 6:497–507. [PubMed: 16799470]
19. Roozendaal R, Carroll MC. Complement receptors CD21 and CD35 in humoral immunity. Immunol. Rev. 2007; 219:157–166. [PubMed: 17850488]
20. Chtanova T, et al. Dynamics of Neutrophil Migration in Lymph Nodes during Infection. Immunity. 2008
21. Farr AG, Cho Y, De Bruyn PP. The structure of the sinus wall of the lymph node relative to its endocytic properties and transmural cell passage. Am. J. Anat. 1980; 157:265–284. [PubMed: 7405871]
22. Prigozhina NL, Waterman-Storer CM. Protein kinase D-mediated anterograde membrane trafficking is required for fibroblast motility. Curr. Biol. 2004; 14:88–98. [PubMed: 14738729]
23. Wulfing C, Davis MM. A receptor/cytoskeletal movement triggered by costimulation during T cell activation. Science. 1998; 282:2266–2269. [PubMed: 9856952]
24. Moss WC, Irvine DJ, Davis MM, Krummel MF. Quantifying signaling-induced reorientation of T cell receptors during immunological synapse formation. Proc. Natl. Acad. Sci. U. S. A. 2002; 99:15024–15029. [PubMed: 12415110]
25. Engstler M, et al. Hydrodynamic flow-mediated protein sorting on the cell surface of trypanosomes. Cell. 2007; 131:505–515. [PubMed: 17981118]
26. Kabashima K, et al. Intrinsic Lymphotoxin-beta Receptor Requirement for Homeostasis of Lymphoid Tissue Dendritic Cells. Immunity. 2005; 22:439–450. [PubMed: 15845449]
27. Wang Y, et al. Antigen persistence is required for somatic mutation and affinity maturation of immunoglobulin. Eur. J. Immunol. 2000; 30:2226–2234. [PubMed: 10940914]
28. Hannum LG, Haberman AM, Anderson SM, Shlomchik MJ. Germinalcenter initiation, variable gene region hypermutation, and mutant B cell selection without detectable immune complexes on follicular dendritic cells. J. Exp. Med. 2000; 192:931–942. [PubMed: 11015435]
29. Brady LJ. Antibody-mediated immunomodulation: a strategy to improve host responses against microbial antigens. Infect. Immun. 2005; 73:671–678. [PubMed: 15664904]
30. Getahun A, Heyman B. How antibodies act as natural adjuvants. Immunol. Lett. 2006; 104:38–45. [PubMed: 16364455]
31. Song H, Nie X, Basu S, Cerny J. Antibody feedback and somatic mutation in B cells: regulation of mutation by immune complexes with IgG antibody. Immunol. Rev. 1998; 162:211–218. [PubMed: 9602366]

32. Ehrenstein MR, O'Keefe TL, Davies SL, Neuberger MS. Targeted gene disruption reveals a role for natural secretory IgM in the maturation of the primary immune response. Proc. Natl. Acad. Sci. U. S. A. 1998; 95:10089–10093. [PubMed: 9707605]
33. Boes M, et al. Enhanced B-1 cell development, but impaired IgG antibody responses in mice deficient in secreted IgM. J. Immunol. 1998; 160:4776–4787. [PubMed: 9590224]
34. Hadjantonakis AK, Macmaster S, Nagy A. Embryonic stem cells and mice expressing different GFP variants for multiple non-invasive reporter usage within a single animal. BMC Biotechnol. 2002; 2:11. [PubMed: 12079497]
35. Schaefer BC, Schaefer ML, Kappler JW, Marrack P, Kedl RM. Observation of antigen-dependent CD8+ T-cell/ dendritic cell interactions in vivo. Cell. Immunol. 2001; 214:110–122. [PubMed: 12088410]
36. Kitamura D, Roes J, Kuhn R, Rajewsky K. A B cell-deficient mouse by targeted disruption of the membrane exon of the immunoglobulin mu chain gene. Nature. 1991; 350:423–426. [PubMed: 1901381]
37. De Togni P, et al. Abnormal development of peripheral lymphoid organs in mice deficient in lymphotoxin. Science. 1994; 264:703–707. [PubMed: 8171322]
38. Futterer A, Mink K, Luz A, Kosco-Vilbois MH, Pfeffer K. The lymphotoxin beta receptor controls organogenesis and affinity maturation in peripheral lymphoid tissues. Immunity. 1998; 9:59–70. [PubMed: 9697836]
39. Molina H, et al. Markedly impaired humoral immune response in mice deficient in complement receptors 1 and 2. Proc. Natl. Acad. Sci. U. S. A. 1996; 93:3357–3361. [PubMed: 8622941]
40. Barnden MJ, Allison J, Heath WR, Carbone FR. Defective TCR expression in transgenic mice constructed using cDNA-based alpha- and beta-chain genes under the control of heterologous regulatory elements. Immunol. Cell Biol. 1998; 76:34–40. [PubMed: 9553774]
41. Crocker PR, Gordon S. Mouse macrophage hemagglutinin (sheep erythrocyte receptor) with specificity for sialylated glycoconjugates characterized by a monoclonal antibody. J. Exp. Med. 1989; 169:1333–1346. [PubMed: 2926328]
42. Paus D, et al. Antigen recognition strength regulates the choice between extrafollicular plasma cell and germinal center B cell differentiation. J. Exp. Med. 2006; 203:1081–1091. [PubMed: 16606676]
43. Carroll RC, et al. Dynamin-dependent endocytosis of ionotropic glutamate receptors. Proc. Natl. Acad. Sci. U. S. A. 1999; 96:14112–14117. [PubMed: 10570207]
44. Vandesompele J, et al. Accurate normalization of real-time quantitative RT-PCR data by geometric averaging of multiple internal control genes. Genome Biol. 2002; 3 RESEARCH0034.
45. Valledor AF, Borras FE, Cullell-Young M, Celada A. Transcription factors that regulate monocyte/ macrophage differentiation. J. Leukoc. Biol. 1998; 63:405–417. [PubMed: 9544570]
46. Phan TG, et al. B cell receptor-independent stimuli trigger immunoglobulin (Ig) class switch recombination and production of IgG autoantibodies by anergic self-reactive B cells. J. Exp. Med. 2003; 197:845–860. [PubMed: 12668643]
47. Smith-Gill SJ, Lavoie TB, Mainhart CR. Antigenic regions defined by monoclonal antibodies correspond to structural domains of avian lysozyme. J. Immunol. 1984; 133:384–393. [PubMed: 6202787]
48. Okada T, et al. Antigen-engaged B cells undergo chemotaxis toward the T zone and form motile conjugates with helper T cells. PLoS Biol. 2005; 3:e150. [PubMed: 15857154]

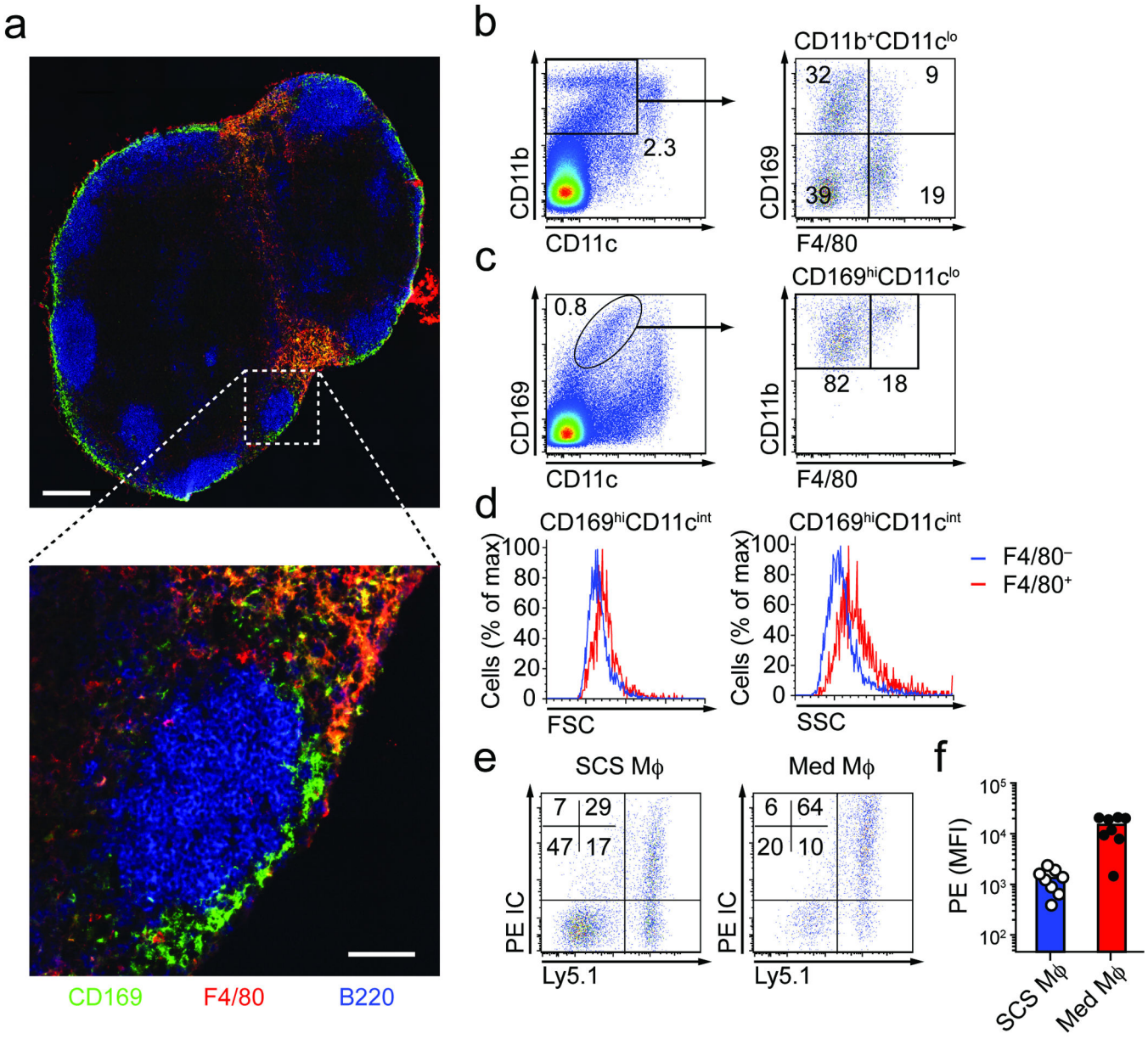

Figure 1. Isolation and identification of SCS macrophages

(a) Mosaic tiled fluorescent microscopy of inguinal LN stained with mAbs to CD169 (green), F4/80 (red) and B220 (blue) to identify SCS and medullary macrophages in situ. Scale bar indicates 200 μm. Inset scale bar indicates 50 μm. Data are representative of 3 experiments. **(b)** and **(c)** Flow cytometric analysis of the same single cell suspension of protease-digested peripheral LNs stained with mAbs to CD11b, CD11c, CD169 and F4/80. **(b)** $CD11c^{hi}$ classical DCs can be distinguished from $CD11b^{+}$ $CD11c^{lo}$ macrophages which can be further resolved into four subpopulations based on CD169 and F4/80. **(c)** Alternative gating strategy showing $CD169^{hi}CD11c^{lo}$ cells comprise $CD11b^{+}$ cells which are either $F4/80^{-}$ SCS macrophages or $F4/80^{+}$ medullary macrophages. **(d)** Forward and side scatter profiles of SCS and medullary macrophages gated as in **(c)**. **(e)** and **(f)** PE-IC capture by

SCS and medullary macrophages 2 hours after PE injection. **(b)–(d)** Data are representative of more than 5 experiments. **(e)** Representative pseudocolor plots from 3 experiments of PE-IC capture by $CD169^{hi}CD11c^{int}F4/80^{-}$ SCS and $CD169^{hi}CD11c^{int}F4/80^{+}$ medullary macrophages. $Ly5.2^{+}$ cells serve as ex vivo mixing controls. Numbers indicate the percentage of cells in each quadrant. **(f)** Graph of pooled data from 3 experiments, n = 5 mice, showing PE mean fluorescence intensity (MFI) of medullary macrophages and SCS macrophages 2 hours after PE injection.

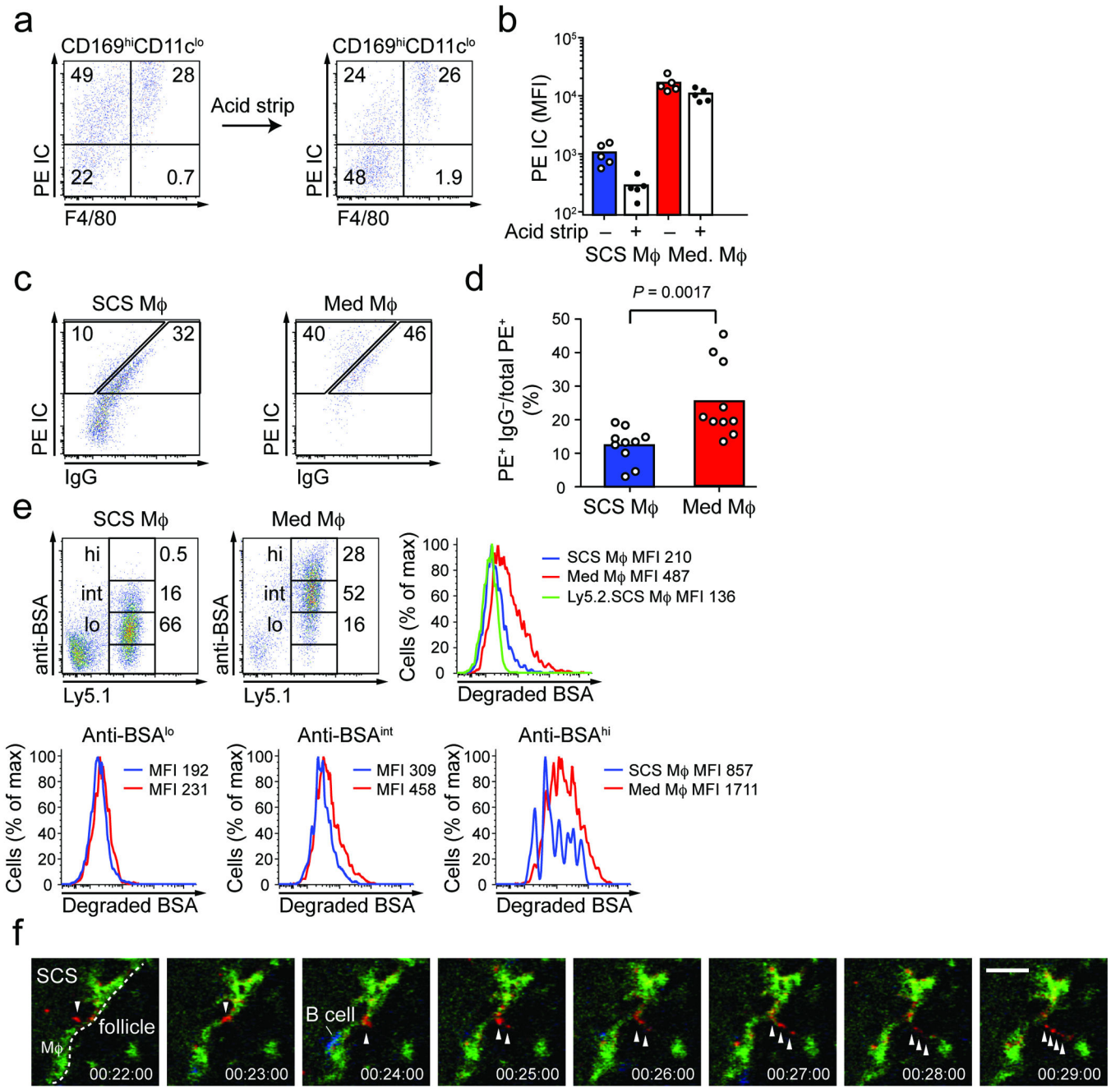

Figure 2. SCS macrophages are poorly endocytic and poorly degradative

(a) and **(b)**. Effect of acid stripping on macrophage retention of ICs. **(a)** PE and PE-specific rabbit IgG was injected to generate PE-ICs *in vivo* and macrophages isolated from draining lymph nodes 4 hours later. Representative pseudocolor plots from 3 experiments show flow cytometric analysis of CD169^{hi} CD11c^{lo} cells before and after acid stripping. **(b)** Graph shows a pool of MFI data for F4/80^{-} (SCS) and F4/80^{+} (medullary) cells where circles indicate individual LNs and bars indicate mean (3 experiments, n= 3 mice). **(c)** and **(d)** Measurement of IC internalization. **(c)** Cells prepared as in **(a)** were surface stained with anti-rabbit IgG to detect PE^{+} IgG^{-} cells. Representative pseudocolor plot from 6

experiments shows detection of PE-IC and rabbit IgG on $CD169^{hi}CD11c^{lo}F4/80^{-}$ SCS and $CD169^{hi}CD11c^{lo}F4/80^{+}$ medullary macrophages. **(d)** Graph of % PE^{+} IgG^{-} cells represents pooled data from 6 experiments, n = 6 mice. Numbers in **(a)** and **(c)** indicate percentage of cells in each gate. **(e)** *In vivo* endocytosis assay. Representative pseudocolor plots from 3 experiments shows gating for SCS and medullary macrophages with low (lo), intermediate (int) and high (hi) amounts of *in vivo* generated BSA-anti-BSA ICs 4 hours after DQ Green BSA injection. $Ly5.2^{+}$ cells serve as a negative control. Overlay histogram shows amount of BSA degradation by SCS and medullary macrophages with the same level of BSA-anti-BSA ICs. **(f)** Time lapse-images from intravital two-photon microscopy shown in the first movie in Supplementary Movie 1 online showing capture, disaggregation and unidirectional transport of discrete bright red PE-ICs along the cellular process of a SCS macrophage labeled green with CD169-specific mAb. Time stamp is in hh:mm:ss. Scale bars represent 10 μm.

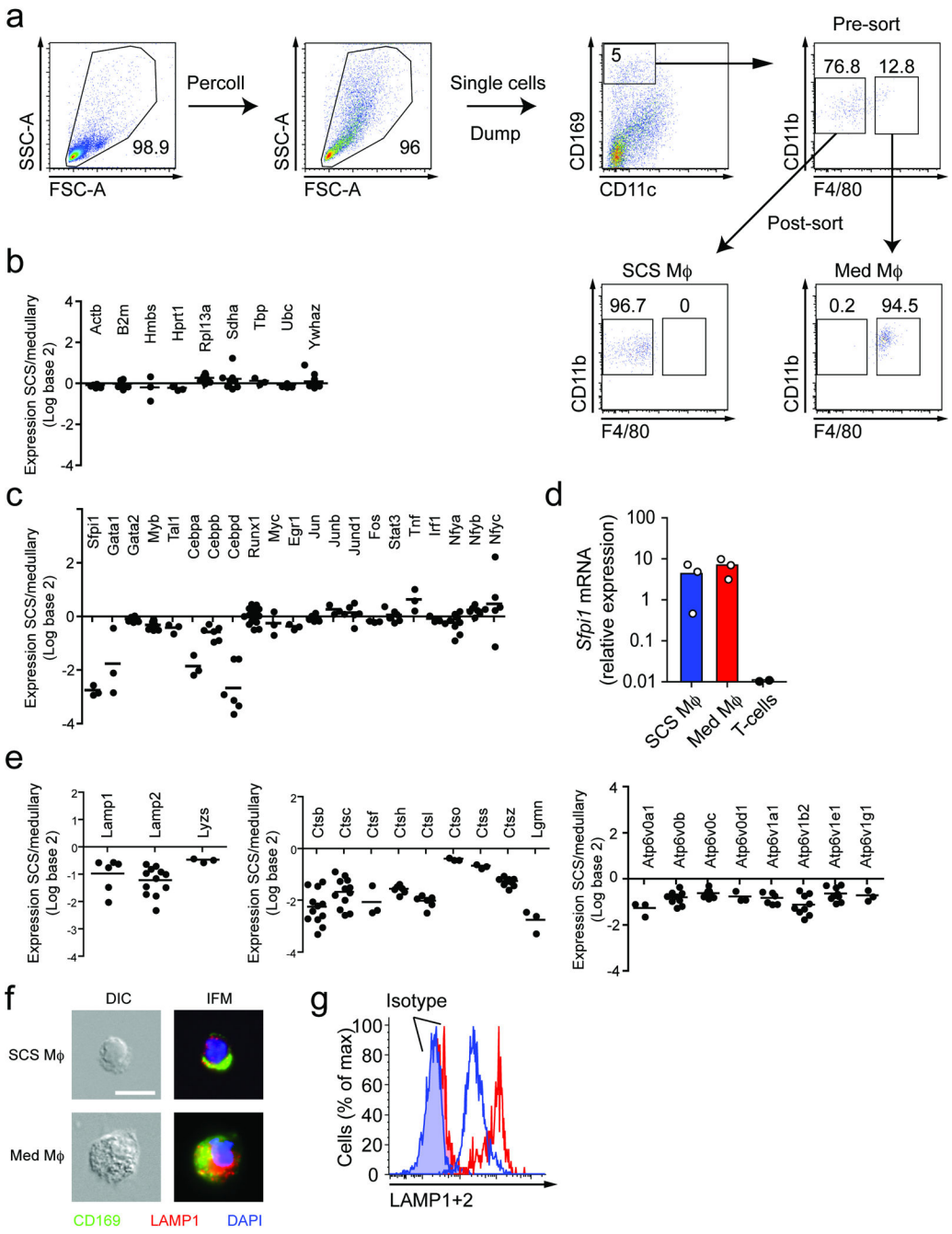

Figure 3. SCS macrophages express low levels of lysosomal enzymes

(a) Purification of SCS and medullary macrophages. Single cell suspensions of protease-digested peripheral LNs were enriched for large low density cells by Percoll density gradient. Single DAPI$^-$ live cells were gated and B220$^+$, CD4$^+$, CD8$^+$ cells dumped. CD169^{hi}CD11c^{lo}CD11b$^+$F4/80$^-$ cells were sorted as SCS and CD169^{hi}CD11c^{lo}CD11b$^+$F4/80$^+$ cells were sorted as medullary macrophages. Numbers indicate the percentage of cells in the gates shown. Pseudocolor plots are representative of 3 experiments, n = 10–15 mice for each sort. **(b), (c)** and **(e)** Comparison of the gene

expression profiles of purified SCS and medullary macrophages showing **(b)** housekeeping genes, **(c)** macrophage transcription factors **(e)** lysosomal proteins, proteases and vacuolar ATPases. Each data point represents an independent experiment (three Affymetrix microarray experiments in total). In some cases there were multiple probe-sets for individual genes and hence more than 3 data points are shown. **(d)** Q-PCR analysis showing expression of *Sfpi1* (PU.1) relative to housekeeping gene *Hprt1* by purified SCS and medullary macrophages. T-cells serve as negative controls. Each data point represents one experiment. **(f)** Microscopy of purified SCS and medullary macrophages showing cell size and granularity by differential interference contrast microscopy (DIC, left panels), and immunofluorescence microscopy (IFM) to detect CD169 (green), LAMP-1 (red) and the nucleus (DAPI, blue). **(g)** Intracellular flow cytometric analysis for LAMP-1 and LAMP-2 protein in SCS macrophages (blue histogram) and medullary macrophages (red histogram) compared to isotype control staining. Data in **(f)** and **(g)** are representative of 3 experiments.

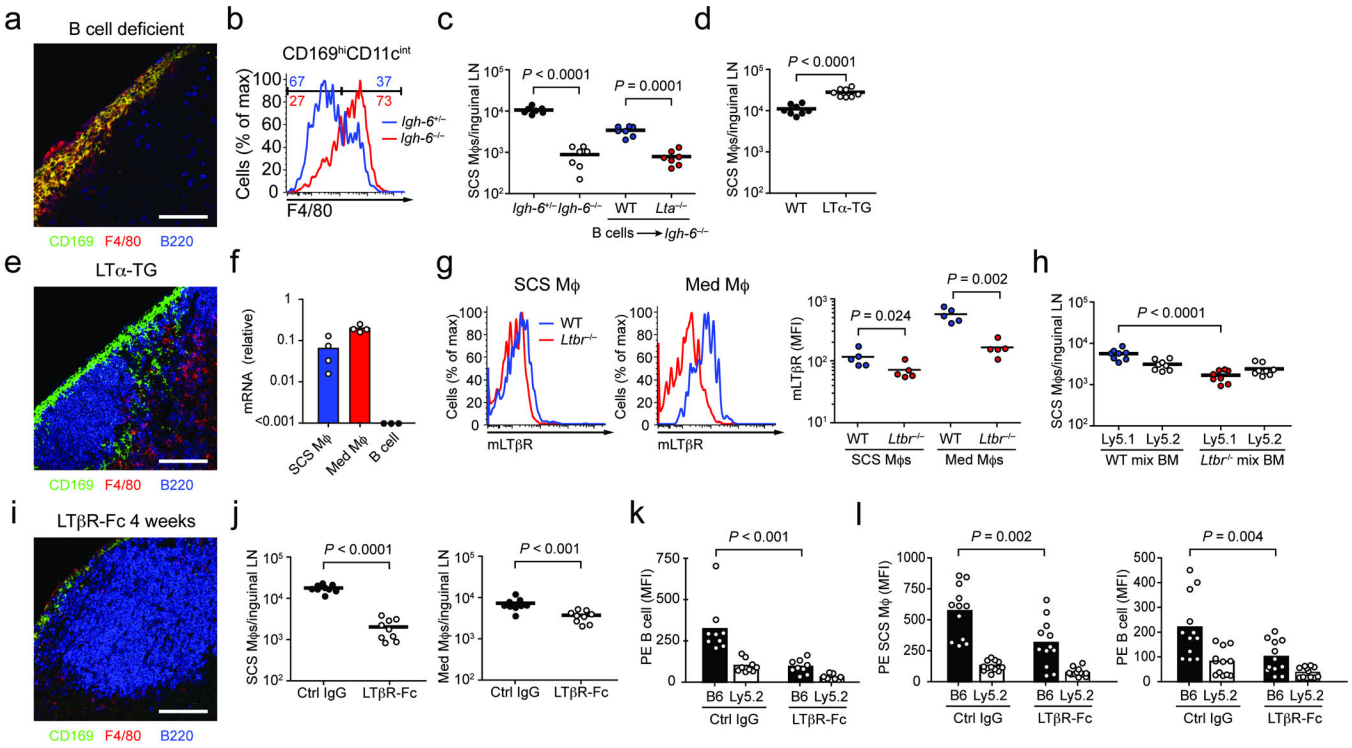

Figure 4. B cell-derived lymphotoxin signaling is required for SCS macrophage differentiation

(a), (b) and **(c)** analysis of SCS macrophages in B cell-deficient *Igh-6*$^{-/-}$ mice. **(a)** Confocal microscopy of paracortical region from the inguinal LN of *Igh-6*$^{-/-}$ mice stained with CD169 (green), F4/80 (red) and B220 (blue). Macrophages lining the SCS are all double positive for CD169 and F4/80. **(b)** Overlay histogram of flow cytometric analysis showing F4/80 expression by CD169^{hi}CD11c^{lo} of inguinal LN from *Igh-6*$^{-/-}$ and *Igh-6*$^{+/-}$ littermates. **(a)** and **(b)** Data are representative of 3 experiments. **(c)** Enumeration of SCS macrophages per inguinal LN of *Igh-6*$^{+/-}$, *Igh-6*$^{-/-}$ and *Igh-6*$^{-/-}$ reconstituted with WT or *Lta*$^{-/-}$ B cells. **(d)** Enumeration of SCS macrophages per inguinal LN of WT and LTα transgenic mice. **(c)** and **(d)** Circles indicate individual inguinal LNs (3 experiments, n = 5 mice). **(e)** Confocal microscopy performed as in **(a)** of inguinal LN from LTα transgenic mouse. Data are representative of 3 experiments. **(f)** Q-PCR analysis of LTβR gene expression by purified SCS and medullary macrophages. Each data point represents a single experiment, n = 10–15 mice. B cells serve as negative control. **(g)** Overlay histogram of flow cytometric analysis for surface expression of LTβR by WT (blue) and *Ltbr*$^{-/-}$ (red) SCS and medullary macrophages (left panel). Graph of LTβR MFI (right panel). Data are representative of and pooled from 3 experiments, n = 5 mice. **(h)** Enumeration of SCS macrophages in WT (blue) and *Ltbr*$^{-/-}$ (red) mixed BM chimeras. The Ly5.2 congenic control is shown in white. Circles indicate individual inguinal LNs (3 experiments, n = 5 mice). *(i)* and *(j)* Mice were treated with LTβR-Fc or control human IgG for 4 weeks and lymph nodes stained to detect SCS and medullary macrophages *in situ* **(i)** or by flow cytometry **(j)**. Left graph shows the enumeration of SCS macrophages and right panel of medullary macrophages. Circles indicate individual inguinal LNs (3 experiments, n = 6 mice). **(k)** Flow cytometric analysis of PE-IC capture by follicular B cells 2 hours after PE

injection in mice treated for 2 weeks with control IgG or LTβR-Fc. Circles indicate individual inguinal LNs (3 experiments, n = 8 mice). **(l)** Reduced SCS macrophage and B cell IC capture following 3 day LTβR-Fc treatment. Circles indicate individual LNs (3 experiments, n = 8 mice). Scale bars in **(a), (e)** and **(i)** indicate 100 μm.

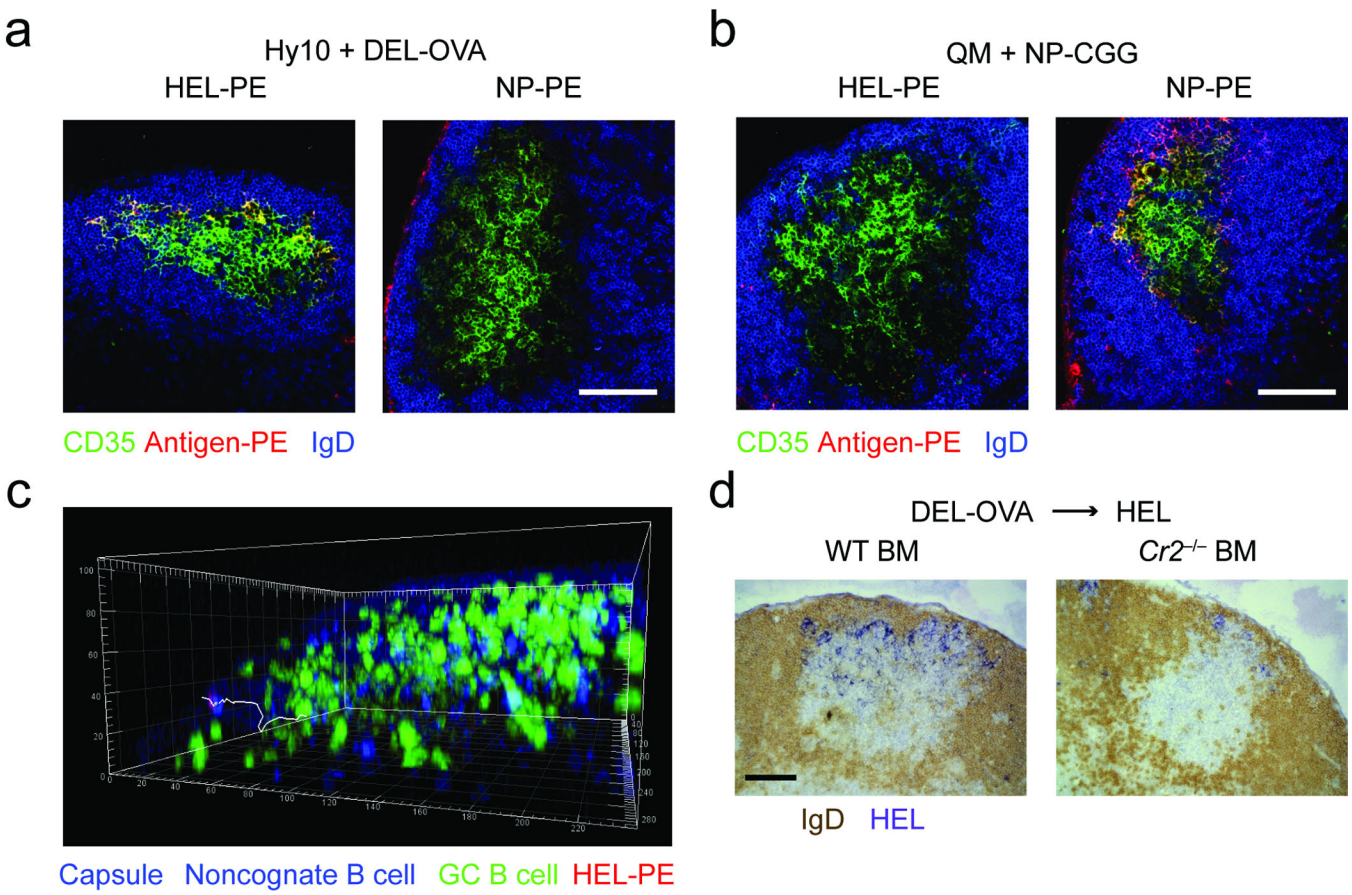

Figure 5. Non-cognate B cells relay antigen opsonized by newly formed antibodies into the GC

(a) Hy10 B cells were adoptively transferred together with OT-II T-cells and immunized with DEL-OVA. Seven days later mice were re-challenged with either cognate HEL-PE (red, left panel) or non-cognate NP-PE (red, right panel). 8 hours after challenge LNs were stained with CD35 (green) and IgD (blue). **(b)** QM B cells were transferred and recipients challenged with NP-CGG. Seven days later mice were rechallenged and analysed as in **(a)**. **(a)** and **(b)** Data are representative of 3 experiments. **(c)** Three-dimensional reconstruction of follicle in $Cr2^{-/-}$ BM chimera 7 days following DEL-OVA immunization, imaged in Supplementary Movie 2 online. The capsule is visible in blue, GC B cells are green and adoptively transferred WT follicular B cells are cyan. HEL-PE was injected 3 hours before the lymph node was harvested and imaged. White track represents movement of a HEL-PE IC^{+} CFP^{+} B cell. **(d)** Immunohistochemical assessment of antigen distribution in WT and $Cr2^{-/-}$ BM chimeras. Mice were challenged 7 days after immunization with HEL-OVA and 8 hours later draining LNs were stained for HEL (blue) and IgD (brown). Data are representative of 3 experiments. Scale bars **(a), (b)** and **(d)** indicate 100 μm. Co-ordinates in **(c)** indicate distance in μm.

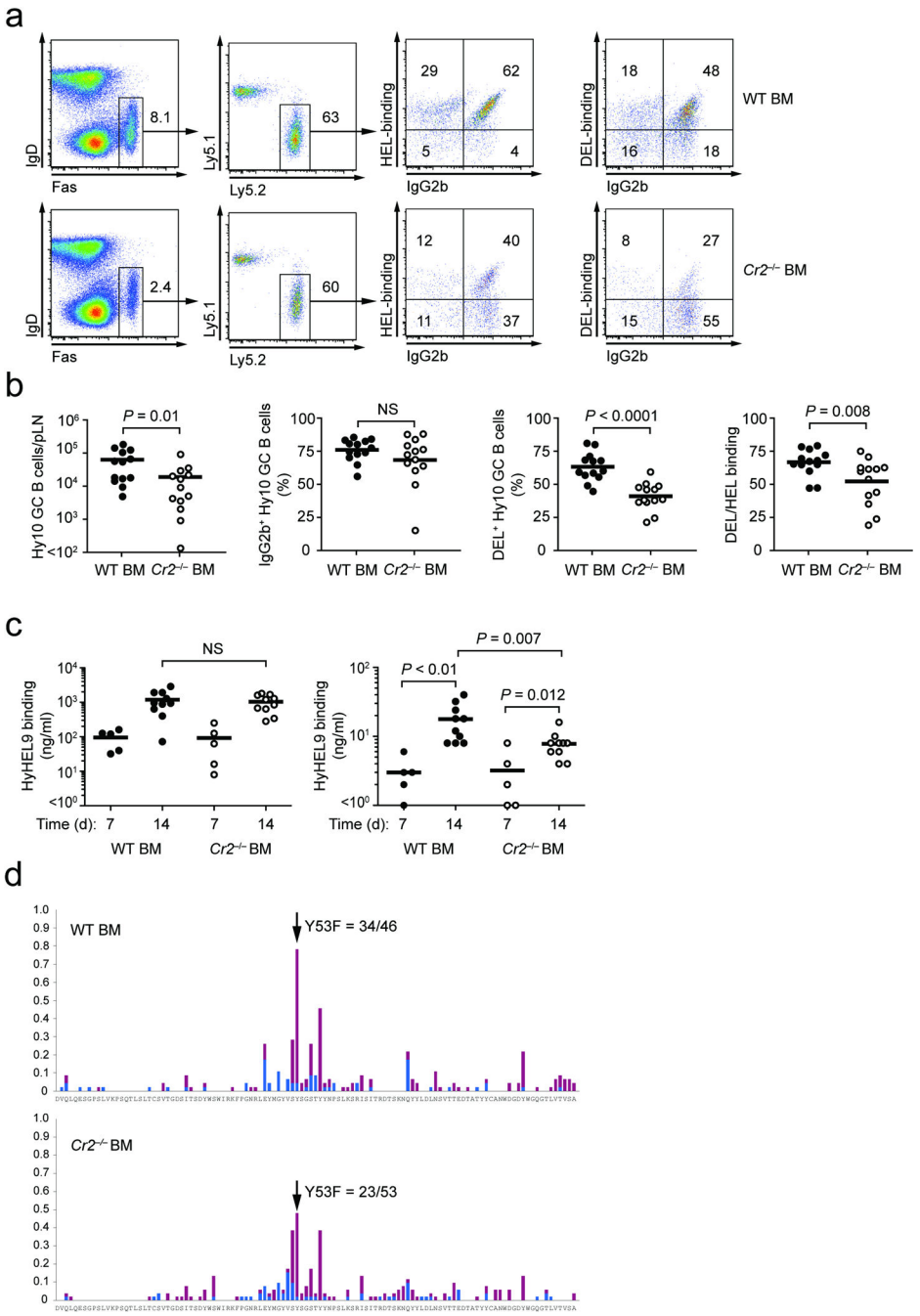

Figure 6. IC relay into the GC drives affinity maturation

Wild-type mice that had been reconstituted with *Cr2*$^{-/-}$ or WT BM received Hy10 B cells and OT-II T-cells on day-1. Mice were immunized on day 0 with the low affinity antigen DEL-OVA in adjuvant and analysed on day 7 and 14. **(a)** Flow cytometric analysis of draining LNs for Ly5.1, Ly5.2, Fas, IgD, HEL-binding BCR and IgG_{2b}. GC B cells are identified as Fas^{hi} IgD^{lo} and transferred cells as Ly5.2^{+}. Middle- and far-right plots show HEL-binding and DEL-binding BCR and IgG_{2b} gated on donor-derived Hy10 B cells as indicated. Numbers indicate frequencies of cells in the gates or quadrants. Data are

representative of 4 experiments. **(b)** Enumeration of GC response, class switching to IgG_{2b} and affinity maturation (DEL-binding) on day 14 using the gates shown in **(a)**. Circles indicate individual LNs (4 experiments, n = 9 mice). **(c)** Serum anti-HEL and anti-DEL Igκ ELISA for low and high affinity antibodies, respectively, on day 7 (2 experiments, n = 5) and 14 of the response (4 experiments, n = 9 mice). HyHEL9 mAb which recognises a distinct epitope from Hy10 B cells was used to construct a standard curve for quantitation of antibody levels. **(d)** Somatic hypermutation (SHM) data on day 14. Mice were immunized as above and donor-derived GC B cells sorted on day 14 for single-cell PCR and sequence analysis. Arrow indicates the position of Y53. Replacement mutations are in red and silent mutations in blue bars. Frequency of Y53F mutations is significantly higher for WT (34/46) than $Cr2^{-/-}$ BM chimera recipients (23/53, $P = 0.002$, Fischer's exact test). Sequence data are from a single sorting experiment.